Gluons moving sideways and how to find them: Transverse momentum dependent parton distributions from the $J/\psi + \gamma$ final state

Marcin Jastrzebski

Supervised by: Prof. Vakhtang Kartvelishvili
Lancaster University, Physics Department

Abstract

The transverse momenta of gluons can be described using parton distribution functions (PDFs). They affect many processes at the LHC, yet little experimental information about them has been extracted to date. The $J/\psi + \gamma$ final state has been recognised as their potential probe at currently available experiments. This work investigates the effects of acceptance cuts required by the ATLAS detector on $J/\psi+\gamma$ data, using simulated events. The transverse momentum distribution of the final state contains information about a gluon PDF called f_1^g. This information is shown to be lost after the detector cuts are applied. Properties of related final state variables are studied and other ways of obtaining f_1^g are considered. Promising results arise from choosing a special coordinate system to describe the transverse momentum in. A measurement of a new variable in the 2015 ATLAS data is proposed as a method of finding f_1^g. Preliminary predictions for extending the analysis to data from the full LHC Run 2 are described. The method appears to remain relevant for the larger data set as well.

Contents

1 Introduction

The Large Hadron Collider (LHC) at CERN has been the biggest and most powerful particle accelerator for over a decade [1, 2], producing copious amounts of research and deepening our understanding of fundamental particles. It will continue to do so with the upcoming Run 3 (2021) [3] and the future High Luminosity upgrade (2027) [4].

The LHC accelerates (mainly) protons but the high energy collisions actually come from the interactions between the protons' constituents. Most interactions originate from the fusion of sub-proton particles called *gluons* [5]. By understanding how these gluons are distributed inside of their parent protons we can not only have a more complete picture of the inside of the protons but also better describe the products of their collisions.

Information about the internal structure of protons is encoded in parton distribution functions (PDFs). In Section 2 we cover the role they play in high energy collisions and why the transverse

momentum of colliding particles needs to be taken into account to properly describe various observable properties of final states. We explain why little information has so far been extracted about gluons in this context.

The goal of this paper is to introduce a way of obtaining one of these transverse momentum dependent parton distribution functions (TMD PDFs). The process which could be used for this purpose is described in Section 2.2. ATLAS detector acceptance cuts (covered in Sec. 2.3) play a big role in obscuring the results. The details of their effects can be found in Sec. 3, where we describe our analysis. Fortunately, a promising way of getting past those obstacles is found and reported in Sec. 3.4. In the future, larger data sets could be used for this study. Some predictions and tentative results have been compiled in Sec. 4. A summary of the main findings can be found in Sec. 5.

2 Background

2.1 Hadronic collisions at high energy

One cannot usually talk about the collisions of protons as if they were uniform, structureless objects. When the energies in the collision are high enough, the protons are torn apart and their constituents can reconfigure themselves to create new particles, not accessible to us otherwise. These can then be studied to give us insight into the fundamental physics allowing for their existence. To know what is hidden inside the proton is to know how this process of creation begins.

We often refer to hadrons by their *static* composition. That is, our proton can be identified with an up-up-down (uud) configuration of quarks, the π^+ is referred to as a $u\bar{d}$ and even some more exotic particles can be described this way, like one of the recently observed tetraquarks, $Z_{cs}(4000)^+$ which corresponds to $c\bar{c}u\bar{s}$ [6][1]. Quantum Chromodynamics however, tells us that what holds these hadronic states together is the strong force, mediated by particles called *gluons*. They have a unique property of being able to produce (couple to) other gluons. They can also radiate quark-antiquark pairs. Altogether this means that a proton will contain a whole quark-gluon *sea* in addition to the *valence uud* quarks. The valence quarks are what determines the static properties of a hadron, like its quantum numbers and rest mass [7, 8]. If we wish to understand collisions of protons at high energies however, we need to include the effects of the quark-gluon sea into the picture. As mentioned before, the gluon interactions tend to, in fact, dominate proton-proton collisions at the LHC. This motivates the quest to understand the properties of gluon distributions.

2.1.1 Factorisation and parton distribution functions

Why hadrons are held together by gluons can be understood via the so-called *colour confinement* [8]. It arises from the behaviour of the strong force coupling coefficient [9]. At low energies (large

[1]This does not define hadrons *uniquely*, as excited states of the same quark configuration are considered separate particles.

distances), the strong coupling becomes very high and prevents individual quarks from ever being observed in isolation (they have to form a hadron - a "colourless" state). Because of its value diverging to infinity, the coupling can no longer be described using perturbative QCD beyond a scale $\Lambda_{QCD} \approx 100\,\mathrm{MeV}$ [10]. It means there is no good recipe for calculating the strength of gluon interactions on length scales corresponding to the size of hadrons [9]. We need to know what happens at these length scales if we are to properly describe high energy collisions. An important tool that allows one to handle this problem is called *factorisation*. What is being factorised are the two scales - the high energy scale where perturbative measures can be used and the large distance scale which corresponds to the picture of the whole inside of the hadron [11].

This procedure will not be possible for all processes [12]. Proving it for a given process is highly nontrivial [13] and involves many subtleties. Processes which can exploit this method are expected to not have much interference between the initial parton collision (the "hard scattering") and the formation of hadrons [11]. Figure 1 shows this idea for a general hadron-hadron collision $h_1 + h_2 \to C + D + X$, where C and D are some final state particles produced in the hard process and $X_1 + X_2 = X$ are all other products of the collision (coming from the break-up of the hadrons, for example).

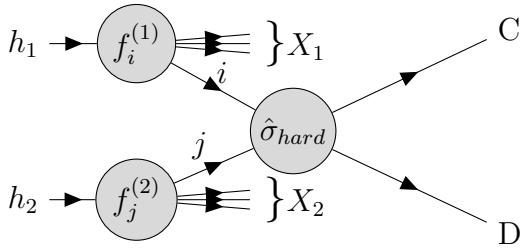

Figure 1: Factorisation in a hadron-hadron collision at high energy. Functions $f_k^{(n)}$ represent large scales and $\hat{\sigma}_{hard}$ corresponds to the small scale, producing the final state $C + D$. $X_1 + X_2 = X$ are all other products of the collision.

Mathematically, this means that the cross section for a given process can be found as [14]:

$$\mathrm{d}\sigma \propto \sum_{i,j} \int \mathrm{d}x_1\, \mathrm{d}x_2 f_i^{(1)}(x_1) f_j^{(2)}(x_2)\, \mathrm{d}\hat{\sigma}_{hard}, \tag{1}$$

where $\mathrm{d}\hat{\sigma}_{hard}$ is the calculable part and the functions $f_k^{(n)}(x_n)$ are known as *parton distribution functions* (PDFs). The summation is taken over all possible parton interactions which can result in the final state $C + D$.

PDFs can be obtained from experiment [14] and represent the probability of finding a given parton k with x_n - the momentum fraction of the parent hadron n. An important feature of PDFs is their universality [11]. This means that once a PDF is obtained from a process, it can be used in other processes containing the same type of parton. This makes PDFs powerful tools in understanding

hadronic collisions. The accuracy of any calculation based on QCD depends on the accuracy of the PDFs. At present, they often are the ones limiting the precision of measurements [15], which motivates the need to study them better.

So far we assumed that all the partons move along with the parent hadron, not allowing for any movement in the plane perpendicular to the motion of the parent. This is known as *collinear factorisation*. It is an obvious simplification, ignoring the three-dimensional structure of the momentum in a collision, to which many cross sections can become sensitive [16].

Transverse momentum dependent formalism is an extension of the collinear factorisation. TMD PDFs (also TMDs) take the form: $f_k^{(n)}(x_n) \rightarrow f_k^{(n)}(x_n, \mathbf{k_{nT}})$, where $\mathbf{k_{nT}}$ is the momentum of the parton transverse momentum. They are necessary to describe several transverse momentum spectra, like that of the Z-boson or final states with multiple jets [17]. Gluon TMDs specifically, play a role in the description of cross sections containing the Higgs boson [17] and could even help identify whether the Higgs is a scalar or a pseudoscalar (beyond the Standard Model) particle [18].

2.1.2 TMDs for gluons

There are eight independent gluon TMDs for a proton [19]. Two of those describe gluons relevant to collisions at the LHC (collisions of unpolarised protons) [20]. These are called f_1^g and $h_1^{\perp g}$. The former corresponds to unpolarised gluons whilst the latter is a contribution from linearly polarised gluons.

The two are related by a *positivity bound* [21]:

$$\left|h_1^{\perp g}\right| \leq \frac{2M^2}{\mathbf{k}_T^2} f_1^g. \tag{2}$$

Equation 2 is model-independent. Nothing else is currently known about $h_1^{\perp g}$. However, according to [22] the saturation of the positivity bound ($\leq$ becomes $=$) might be a reasonable assumption and several studies [20, 23] use it in their theoretical analysis. This means that the extraction of f_1^g could be very telling of the overall behaviour of gluons in LHC protons.

This report contains analysis of simulated data based on the ATLAS experiment at the LHC. The aim is to show how f_1^g could be extracted from real data for a particular final state. The motivation and background behind using that process is described in Section 2.2. The extraction requires a discussion of detector acceptance effects (See Sec. 2.3), which are shown to give rise to problems in analysing the results. Section 3 gives details of the analysis performed and introduces a way of overcoming the obstacles coming from these acceptance effects. This could result in the future extraction of f_1^g.

2.2 $J/\psi + \gamma$ production

2.2.1 A gluon probe

To be appropriate for the study of TMDs, a process needs to be factorisable and experimentally accessible. These include Semi Inclusive Deep Inelastic Scattering and Drell-Yan processes measurements [24, 25], which currently provide the majority of our experimental knowledge on TMDs. These two processes, unfortunately, are primarily initiated by quark/antiquark interactions and therefore do not hold information about gluon distributions. The current lack of knowledge of gluon TMDs is mainly due to the lack of data on promising process.

A potentially very convenient probe of the gluon TMDs is the back-to-back production of a heavy quark pair in electron-proton collisions $e + p \to e + Q + \bar{Q} + X$. Access to such final states will only be available in future facilities, like the EIC and LHeC [26]. Many currently accessible processes at LHC and experiments like HERA [27] or RHIC [28] suffer from contamination form quark-induced channels or experimental difficulties like large backgrounds or difficulties in observing the final states themselves [29, 30]. Other processes experience breaking of TMD factorisation [26].

A handful of processes with data currently available at the LHC have been proposed [5, 20, 23, 31].

As mentioned previously, factorisation will not hold for all processes within the TMD formalism. One of the requirements is that the transverse momentum q_T of the final state should be much smaller than the hard scale of the process Q, which corresponds to the invariant mass of the final state [20].

This makes two-particle final states much better processes for extraction of TMDs as the two particles can have very high momenta in nearly opposite directions, resulting in a low vector sum. High transverse momenta of individual particles make them easier to observe in a typical, cylindrical detector (See Section 2.3 for details).

The J/ψ $(c\bar{c}) + \gamma$ has been recognised [32] as one of the best final states to probe gluons at proton-proton colliders. First, in leading order, this state can *only* be produced by gluon fusion. Additionally, if one requires both of the products to have significant p_T (separately, total transverse momentum q_T remains small), there is only one process leading to $J/\psi + \gamma$ in the final state. It is shown in Figure 2. This means that we know exactly how the final state is produced and that it is related to the properties of gluons in the collision.

It is important that there is not much activity between this high energy (hard) process and the detection of the two final state particles. We want the particles we observe to "remember" the gluons' properties very well, and any additional interactions on their way to the detectors would obscure that memory. In the loop diagram visualised in Fig. 2, any additional radiation from the gluon is suppressed due to the high mass of the charm quark. Photons can only interact electromagnetically which significantly suppresses its interactions with the products of the interaction (electromagnetic coupling is over 100 times lower than that of the strong force). Even though J/ψ is a hadron, because of its high mass and heavy quark composition, it is expected to interact with the collision remnants much weaker than, say, a pion [32]. When the $c\bar{c}$-pair is produced, it goes readily into the bound state, without any additional strong radiations. The J/ψ decays into light hadrons are

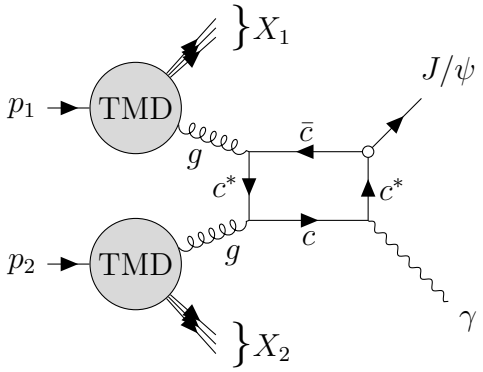

Figure 2: The only leading-order diagram for the production of $J/\psi + \gamma$ in proton-proton collisions when both final state particles are required to have high transverse momenta.

OZI-suppressed [33], meaning it often decays into $\mu^+\mu^-$ which, just like the photon, can no longer contribute further strong interactions. Altogether these properties of the $J/\psi + \gamma$ production make it a very clean probe of gluons hidden within the protons colliding at the LHC.

2.2.2 Where is the transverse momentum?

The introduction of transverse momentum dependence modifies, Eq. 1. For our final state [5]:

$$\frac{\mathrm{d}\sigma}{\mathrm{d}\Omega\,\mathrm{d}^2\,\mathbf{q_T}\,\mathrm{d}Y\,\mathrm{d}Q} \propto \left\{ F_1\mathcal{C}\left[f_1^g f_1^g\right] + \cos 2\phi_{CS}\left(F_{3_a}\mathcal{C}\left[w_{3a} f_1^g h_1^{\perp g}\right] + F_{3_b}\mathcal{C}\left[w_{3b} h_1^{\perp g} f_1^g\right]\right) + \cos 4\phi_{CS} F_4 \mathcal{C}\left[w_4 h_1^{\perp g} h_1^{\perp g}\right]\right\}. \tag{3}$$

Here the F-factors are the calculable part related to the hard process, each term containing an F corresponds to a different type of gluon-gluon collision. The convolutions $\mathcal{C}$ contain information about the distribution functions:

$$\mathcal{C}\left[wfg\right] = \int \mathrm{d}^2\,\mathbf{k}_{aT} \int \mathrm{d}^2\,\mathbf{k}_{bT}\delta^2(\mathbf{k}_{aT} + \mathbf{k}_{bT} - \mathbf{q}_T) w(\mathbf{k}_{aT}, \mathbf{k}_{bT}, \mathbf{q}_T) f(x_a, \mathbf{k}_{aT}^2) g(x_b, \mathbf{k}_{bT}^2), \tag{4}$$

where w are weights which are also calculable and common for all gluon-gluon fusion processes. In collinear factorisation, $h_1^{\perp g}$ is assumed to be 0 (leaving only the F_1-term) in Eq. 3 and $f(x, \mathbf{k_T}) = f(x)\delta^2(\mathbf{k_T})$ in Eq. 4, allowing the two distribution functions to cancel the convolution integrals, reducing to the simple product present in Eq. 1.

The cross section in Eq. 3 is differential in the solid angle $d\Omega = d\cos\theta_{CS} d\phi_{CS}$, in the so-called Collins-Soper frame [34], rapidity Y (See Sec. 3.2), invariant mass of the system Q and most importantly, its transverse momentum $\mathrm{d}^2\,\mathbf{q_T}$. The polarised gluon distribution $h_1^{\perp g}$ is expected to

introduce angular modulations in the Collins-Soper frame [23], but integrating over Ω_{CS} leaves only $F_1\mathcal{C}\left[f_1^g f_1^g\right]$, making the cross section independent of $h_1^{\perp g}$ contributions.

This makes the extraction of f_1^g surprisingly easy in theory and further validates the analysis of $J/\psi + \gamma$ data. The distribution of unpolarised gluons is usually assumed to be Gaussian in their transverse momentum k_T [23, 35]:

$$f_1^g(x, k_T) = \frac{G(x)}{\pi\langle k_T^2\rangle} \exp\left(-\frac{k_T^2}{\langle k_T^2\rangle}\right). \tag{5}$$

$G(x)$ represents the collinear gluon distribution (known) and $\langle k_T^2\rangle$ is the average transverse momentum squared of the gluons.

$\mathcal{C}\left[f_1^g f_1^g\right]$ can then be calculated using Eq. 4 as:

$$\mathcal{C}\left[f_1^g f_1^g\right] = \frac{G(x_1)G(x_2)}{2\pi\langle k_T^2\rangle} \exp\left(-\frac{q_T^2}{2\langle k_T^2\rangle}\right). \tag{6}$$

Combining with Eq. 3 we obtain:

$$\frac{\mathrm{d}\sigma}{\mathrm{d}^2\,\mathbf{q_T}} \propto \exp\left(-\frac{q_T^2}{2\langle k_T^2\rangle}\right), \tag{7}$$

where $\mathrm{d}^2\,\mathbf{q_T} = q_T\,\mathrm{d}q_T\,\mathrm{d}\phi$ and integration over the polar angle ϕ in the transverse plane gives:

$$\frac{\mathrm{d}\sigma}{\mathrm{d}q_T} \propto q_T \exp\left(-\frac{q_T^2}{2\langle k_T^2\rangle}\right). \tag{8}$$

Thus the distribution of events in q_T should follow a fit function:

$$\mathcal{F}(q_T) = p_0 q_T \exp\left(-\frac{(q_T - p_1)^2}{2p_2^2}\right) \tag{9}$$

in the region $q_T \ll Q$ allowing for factorisation. Here p_1 represents a shift which is expected to be 0 but is introduced for later convenience. p_0 is a scaling factor and is not of interest in this analysis and p_2^2 corresponds to $\langle k_T^2\rangle$. By establishing p_2 one should therefore be able to obtain f_1^g from Eq. 5.

2.3 The ATLAS detector acceptance

With the hope of using currently available real-life $J/\psi + \gamma$ data, this analysis uses Monte Carlo (MC) simulations (See Section 3.1) and primarily considers acceptance cuts based on the ATLAS

detector during its operation in 2015. This was the first year of Run 2, when the LHC was operating at the record collision energy of 13 TeV [36].

As mentioned in Sec. 2.2.1, the J/ψ decays to two muons. This means the final state in the detector needs to have two oppositely charged muons fitted to the same production vertex. This, in the real experiment, can be obtained with the `HLT 2mu4 bJpsimumu noL2` trigger, active during the 2015 data-taking. This allows for the extraction of J/ψs with the lowest possible transverse momenta that year [37], increasing the amount of events available. It requires muons to have $p_T > 4\,\text{GeV}$. Muons with lower momenta can be problematic to identify as they often either lose their energy before reaching the Muon Spectrometer (an important step in identifying a muon) [38] or get bent away by the magnetic field present in the detector before traversing all of it [37]. Pseudorapidity measures the deviation from the direction collinear to the beam[2]. It is given by:

$$\eta = \frac{1}{2} \ln \frac{|\mathbf{p}| + p_L}{|\mathbf{p}| - p_L}. \tag{10}$$

The $\mathbf{p}$ denotes the total momentum of the particle and p_L is its momentum along the beam axis. Small $|\eta|$s correspond to trajectories which are close to perpendicular to the beam. The muons are required to fulfil $|\eta| < 2.5$. This cut on the data comes from the geometry of the detector, as areas of higher $|\eta|$ are not covered by the inner tracking detector, the first stage of the detection of charged particles [39]. As for the photons, these are deemed to be reconstructable if their $|\eta| < 2.5$ and $p_T > 5\,\text{GeV}$. The rapidity cut is due to the acceptance of the electromagnetic calorimeter [40], where our photons lose their energy to be detected. Photons identified this way are easier to detect at higher transverse momenta [40].

No detector is ideal and the acceptance cuts discussed here are crucial in faithful reconstruction of the physics occurring in collisions. This unfortunately means that a lot of the events which occur cannot be registered and are effectively lost. This can result in misinterpretation of data or loss of information. In what follows we explain how the detector acceptance cuts spoil the information needed to extract f_1^g as described in Sec. 2.2.2, explore the $J/\psi + \gamma$ final state and propose a new way of obtaining this gluon distribution function, which avoids the distortion from detector effects.

3 Search for TMDs

3.1 Method

To probe the potential of the $J/\psi + \gamma$ final state to reveal the distribution of the gluon transverse momentum, two MC data sets were used. These were simulated with `PYTHIA 8.230` [41] (not by the author).

[2]This is true for massless particles. Massive particles are charectarised by rapidity Y, given by an equation analogous to Eq. 10, but with $|\mathbf{p}|$ replaced with the particle's energy, E. Y and η are equivalent for massless particles (for which $E = |\mathbf{p}|$, with $c = 1$). One can assume the same for highly energetic massive particles where $E^2 = m^2 + p^2 \approx p^2$. We use this approximation for our muons throughout our analysis.

The first data set (`Data Set 1` or `DS1` from now onward) contained around 10^6 events, with no acceptance cuts applied. This sample allowed us to access the "truth" about the gluons' transverse momentum. In other words, if `PYTHIA` simulated gluon TMDs as they occur in nature, the q_T-distribution of the final state in `DS1` would allow us to access f_1^g exactly as described in Section 2.2.2.

`Data Set 2` (`DS2`), the focus of this work, contained roughly 10^7 events and was meant to represent a more realistic data set by implicitly applying p_T acceptance cuts. These were 3.5 GeV for muons and 4 GeV for the photon (3.5/3.5/4 GeV will be the format used from now on), close to the ones we require in our analysis, as described in Sec. 2.3.

The MC samples provide only information about signal data. No background events are used. Actual ATLAS analysis will have to take those into account. There are several sources of background, like the "prompt" production of the J/ψ, directly from the hard process or production of J/ψ in B-hadrons decay. Both of these final states can sometimes contain a photon. There are also events where the J/ψ and γ came from different subprocesses within the same collision or from different collisions in a bunch crossing altogether. Ref. [42] shows methods of subtracting these events from the 2015 ATLAS data set.

Parton distributions are dependent on the collision energy [43], which is the same as the invariant mass of our final state. This means that we should expect some variation of the widths measured at different invariant masses. This motivated us to analyse the data in three mass bins Q. These are summarised in Table 1. They are referred to as Ranges 3, 4 and 5 (for historical reasons).

The rapidity cuts brought the statistics in `DS1` down to about 7.0×10^3, and `DS2` to 3.1×10^5, but produced no significant changes in the shapes of the distributions of interest, contrary to the p_T acceptance cuts applied to `DS2` (See next Section). Applying the additional p_T cuts in `DS2` (3.5/3.5/4 GeV $\rightarrow$ 4/4/5 GeV), required by our analysis, further reduced the number of events by about a half.

Range label	Associated masses (GeV)
3	$15.5 - 22.0$
4	$22.0 - 31.0$
5	$31.0 - 44.0$

Table 1: Three invariant mass ranges of the final state $J/\psi + \gamma$ used to study transverse momenta of gluons.

3.2 Acceptance effects on q_T

As mentioned in Section 2.2.2, a simple measurement of the width of the distribution of q_T of the final state could be traced back to f_1^g. This distribution, along with a fit from Eq. 9 is shown in Fig. 3 for both `DS1` and `DS2` (for the mass range 3). It is worth mentioning that allowing for a shift in the fit to the original distribution introduces significant uncertainty to other parameters (p_0, p_2).

p_1 is still consistent with 0 in the original distribution but a significant non-zero shift is observed in DS2. Additionally, the key parameter $p_2 = \sqrt{\langle k_T^2 \rangle}$, highlighted in red, is affected. The p_T cuts applied result in significant broadening of the distribution. It is not clear how one could obtain p_2 of the "true" distribution just by measuring it in a real experiment.

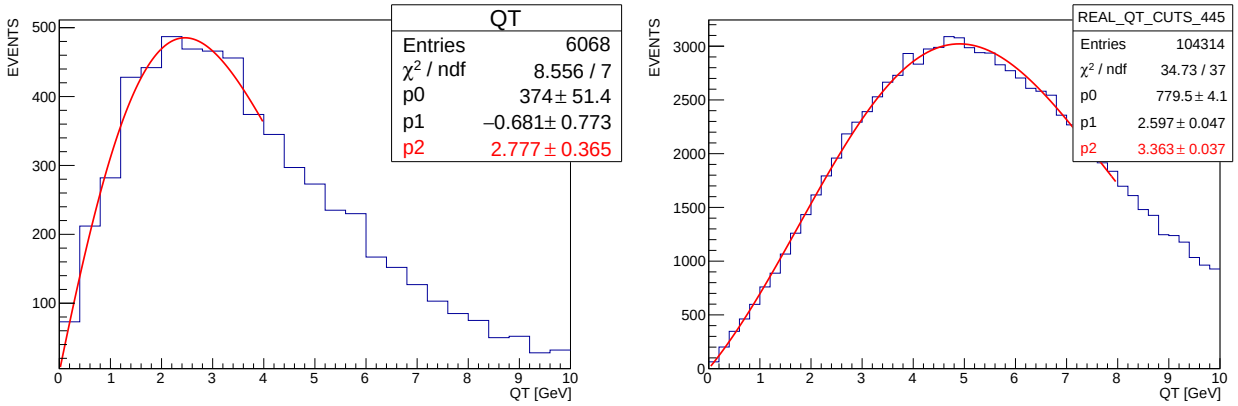

(a) Ideal detector case with no acceptance cuts, "true" distribution.

(b) Realistic detector acceptance cuts applied, distorted distribution.

Figure 3: The distribution of the transverse momentum of the $J/\psi+\gamma$ pair before and after applying acceptance cuts required by the ATLAS detector. Final state mass ranges from 15.5 GeV to 22.0 GeV.

Figure 4 shows a comparison of a more full set of variables, broken down into the three ranges of the invariant mass Q. The first column shows how the events are distributed in Q. The remaining distributions are related to each other. Second column contains q_T, next plotted is q_T^2, which should follow an exponential decay $\propto \exp\left(\frac{-q_T^2}{p_2}\right)$, with the same p_2 as measured in the first column. The last remaining columns plot separately the x and y components of q_T, which are Gaussians around 0 GeV. The width of those, in principle, should also be given by p_2. In DS1, the widths of the x and y components match the widths of q_T and q_T^2. The widths seem not to vary significantly throughout the three mass ranges, although obtaining information from the last range is made difficult due to a limited number of events. The effects of 4/4/5 GeV cuts in DS2 can be seen even more clearly. On top of the broadening happening in all three ranges, q_T^2 in range 3 obtains a dip in the first few bins, visibly losing the exponential dependence expected. The x and y components in this mass range are not well described by a single Gaussian anymore, as the χ^2/N of the fit, where N is the number of degrees of freedom, is around 3. A good fit should not be much bigger than $\chi^2/N \approx 1$. Although the x and y components in the rest of the data can be considered Gaussians, their widths coincide with the widths of q_T and q_T^2 only in the last mass range. The shift in q_T decreases with Q, but does not disappear. The shape of the mass distribution itself should also be noted. Originally, there is a

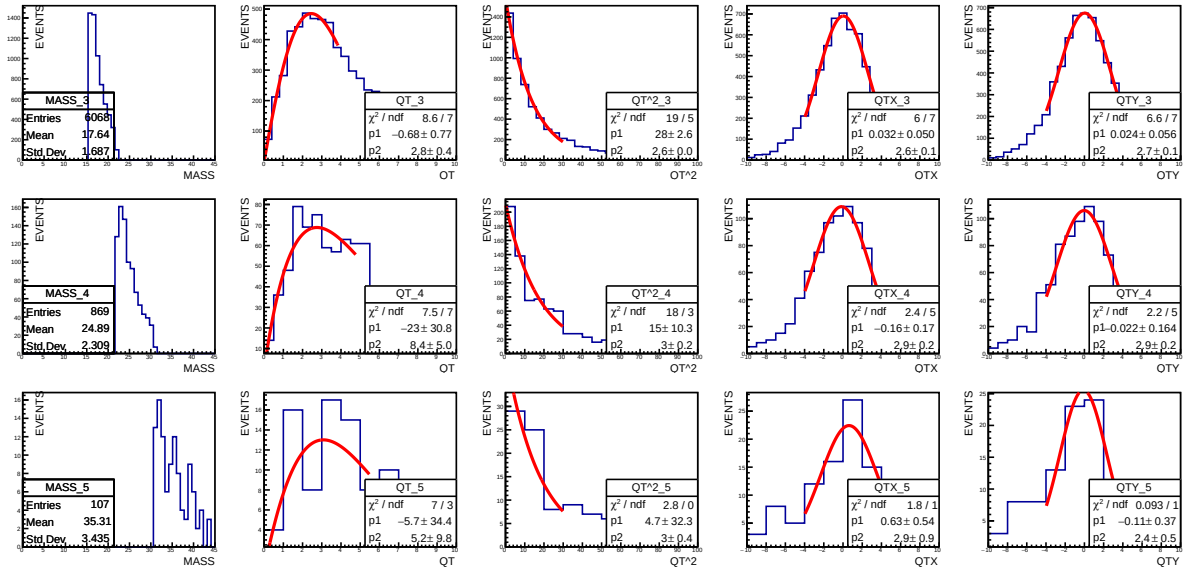

(a) No acceptance cuts applied.

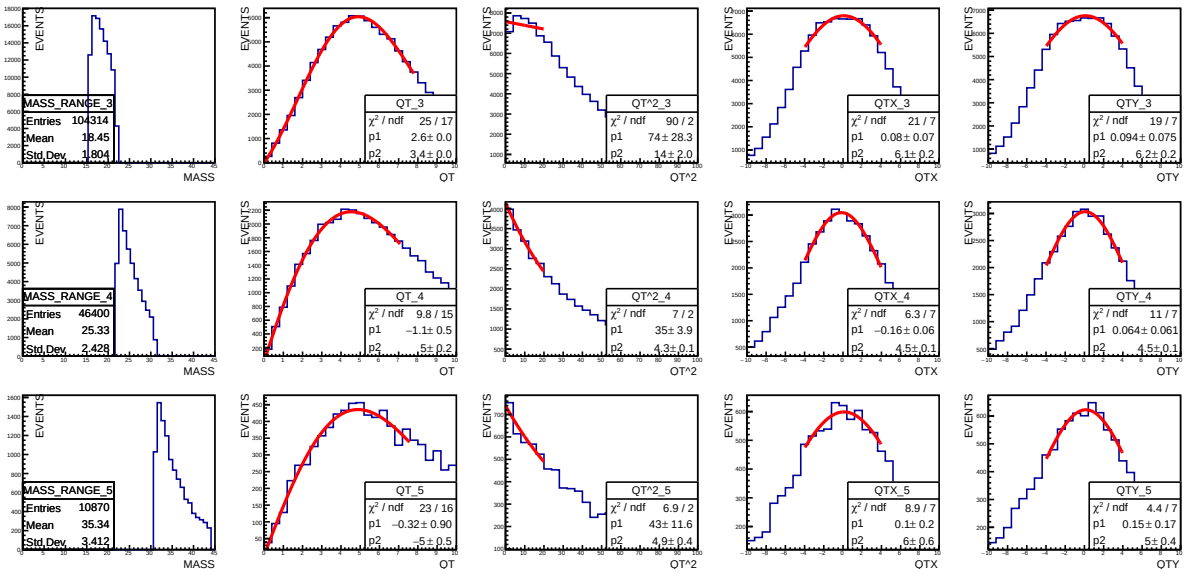

(b) 4/4/5 GeV acceptance cuts applied to final state transverse momenta.

Figure 4: q_T of $J/\psi + \gamma$ and related distributions before and after acceptance cuts required by the ATLAS detector. Three mass ranges are plotted. Horizontal axes given in GeV.

steady decrease in the number of events with mass. After applying acceptance cuts, this distribution has shifted its peak, which has the biggest impact on mass range 3. This likely explains why lower masses suffer the largest deviations from expected behaviour. Overall, the 4/4/5 GeV acceptance cuts have distorted the information about the gluon distributions in a non-trivial way.

As the shape distortion of the distribution comes from applying q_T cuts, it is informative to explore what happens as tighter cuts are applied. We chose to leave the muon cuts untouched and increase the acceptance threshold on the photon. This was motivated by identifying that a 4/4/5 GeV cut is not symmetrical. The lowest J/ψs will have just under 8 GeV, whilst lower momentum photons are allowed. This is unlike the ideal detector case. Figure 5 shows a fit to the y-component of q_T with increasing photon cut $(4 - 16\,\text{GeV})$ for the three mass ranges. None of the ranges reach the original value of $\approx 2.70 \pm 0.07\,\text{GeV}$ at any of the photon cuts. The width of Range 3 gets closest for Photon Cut 8.5 GeV, which indeed corresponds to a more balanced case. Ranges 4 and 5 are less dependent on the photon cut.

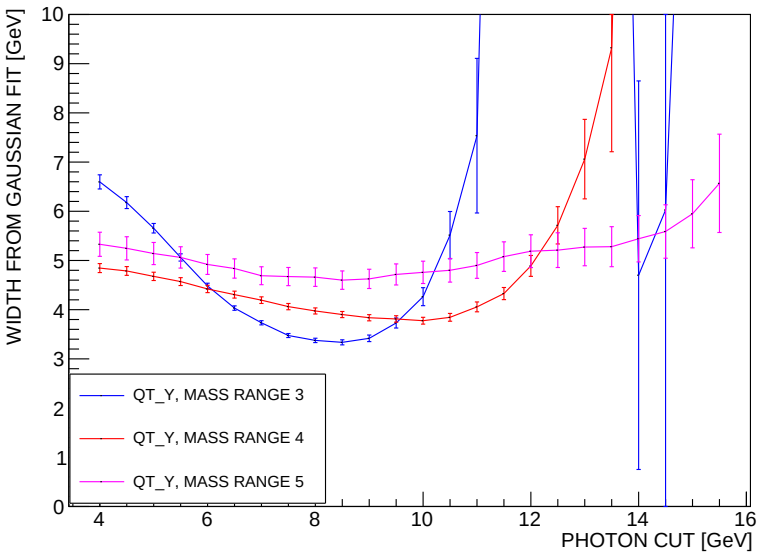

Figure 5: Evolution of the width of the q_{Ty} distribution in the $J/\psi + \gamma$ final state with increasing cut on the photon p_T. Large errors towards higher cuts come from small number of statistics left.

Figure 6 showcases the same breakdown as in Fig. 4 but for cuts 4/4/9 GeV. The peak in mass has now shifted significantly. Gaussianity of x and y components has been restored, but the widths still do not correspond to q_T and q_T^2. An interesting feature of mass range 3 is a bulge emerging around 3 GeV. This indicates statistics are missing from the important, low q_T region.

The analysis of results gathered in this section renders the extraction of f_1^g straight from the distribution of q_T problematic, if not impossible, using ATLAS data. Motivated by this, search

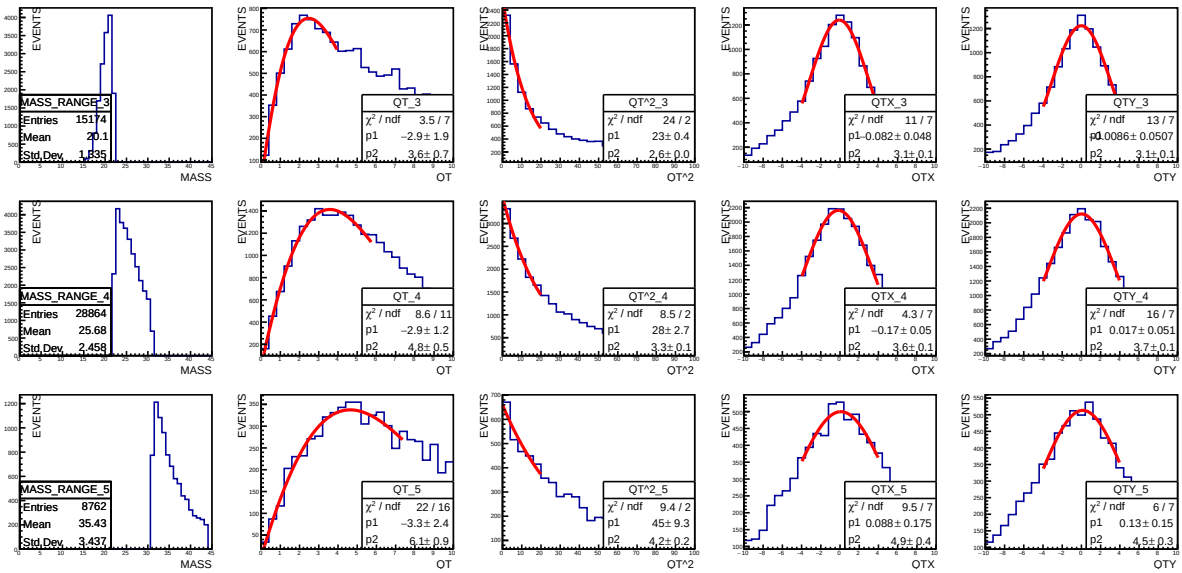

Figure 6: q_T of $J/\psi + \gamma$ and related distributions after acceptance cuts on the photon and J/ψ transverse momenta are made roughly symmetric (4/4/9 GeV). Horizontal axes given in GeV.

for other potential probes of the gluon distributions in the $J/\psi + \gamma$ final state began. Section 3.3 describes a more natural approach to analysing the data along with results from initial attempts of applying it. Promising results follow in Section 3.4.

3.3 Exploring the final state

The non-zero q_T of the $J/\psi + \gamma$ pair which, if small, is generated by the transverse momentum of gluons, defines a direction in each event. From the point of view of the detector this direction is completely random. Acceptance cuts however, are applied *along* the momenta of the two particles in each event. This happens directly for the photon by requiring $p_T(\gamma) > 5\,\text{GeV}$ and indirectly for the J/ψ from $p_T(\mu^{\pm}) > 4\,\text{GeV}$. This means that if we are to study the total momentum of the final state, there are some special directions along which it can be oriented in each event. This will produce a distribution that is less random and possibly contains more information about the underlying physics of the collision.

In this section we explore what happens if we set the x-direction in each event such that it aligns with the direction of either the J/ψ or the photon. This means that, from the point of view of the detector, the definition of x and y changes from event to event.

The original and new distributions are compared in Fig. 7 and 8 for cuts 4/4/5 and 4/4/9 GeV, respectively. The first column contains no rotation with respect to the final state momentum q_T. The distribution is centered around 0 in both x and y as expected from our previous analysis. Worth

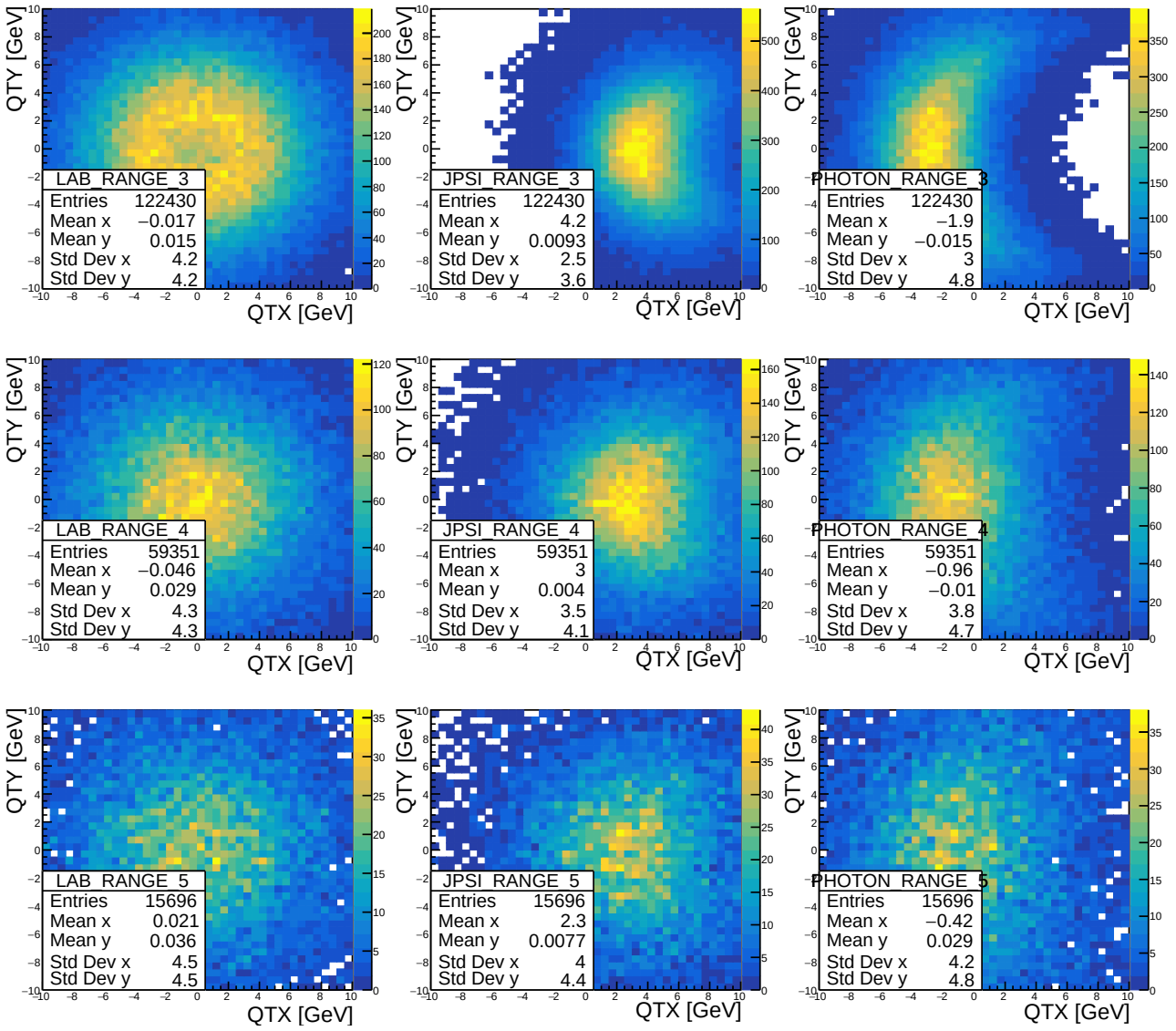

Figure 7: q_T distribution of J/ψ in the transverse plane in the lab frame and two rotated coordinate systems based on the direction of the J/ψ and γ (See text for more explanation). 4/4/5 GeV cuts applied to final state transverse momenta.

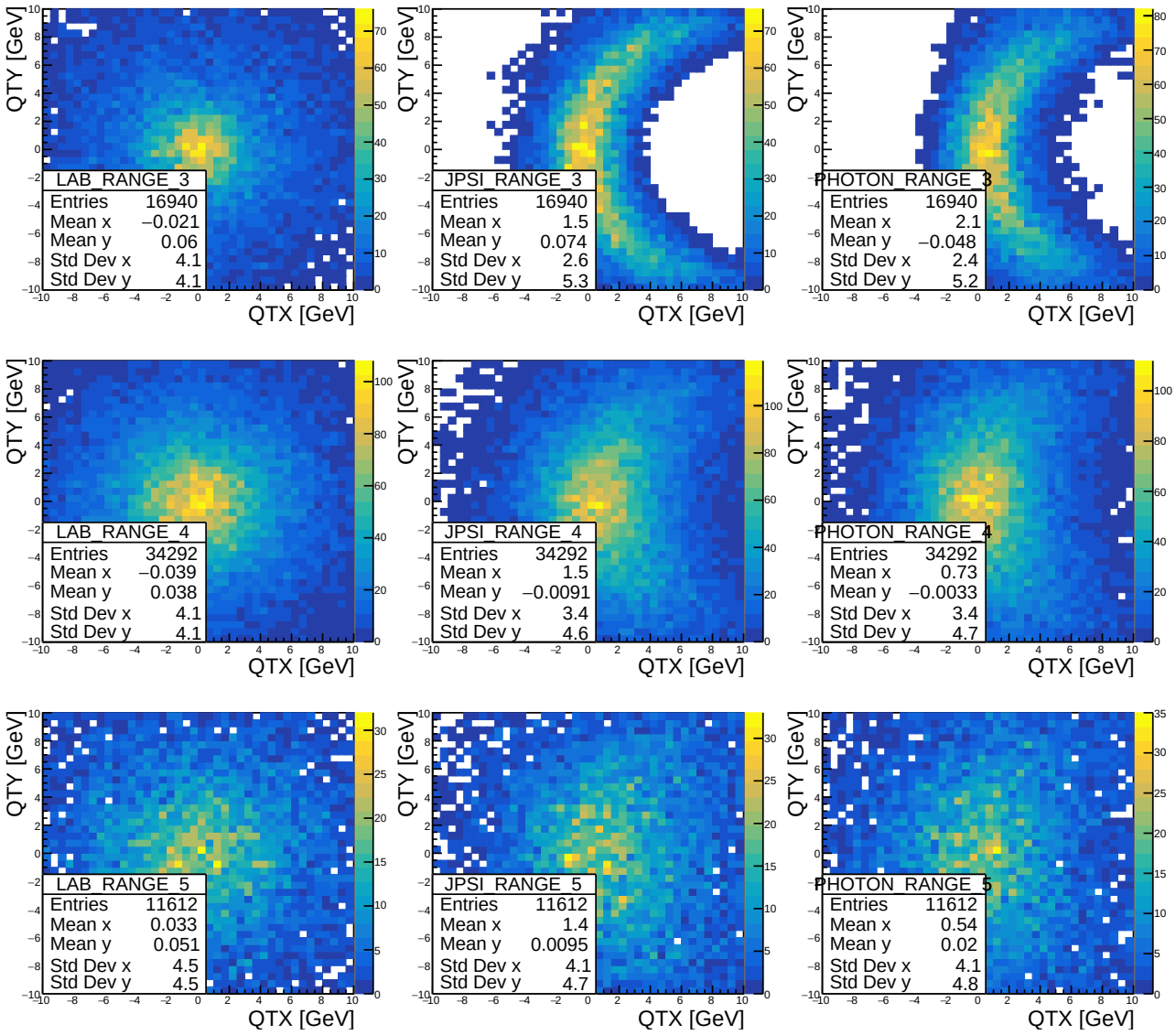

Figure 8: q_T distribution of J/ψ in the transverse plane in the lab frame and two rotated coordinate systems based on the direction of the J/ψ and γ (See text for more explanation). 4/4/9 GeV cuts applied to final state transverse momenta.

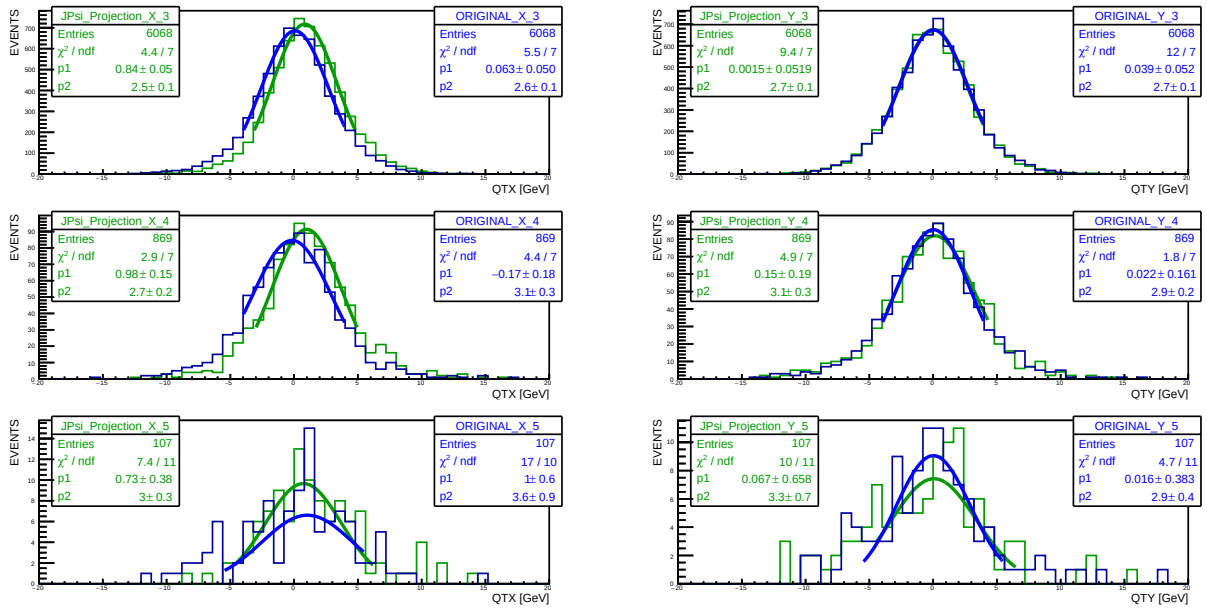

(a) Sample with no acceptance cuts.

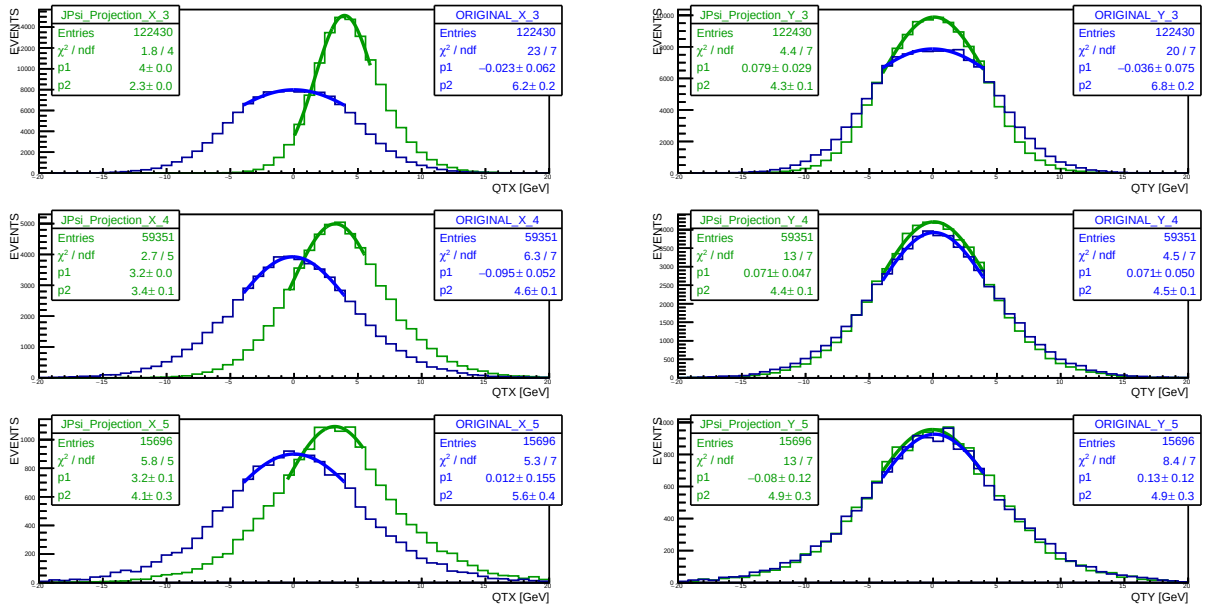

(b) Sample with 4/4/5 GeV cuts applied to final state transverse momenta.

Figure 9: q_{Tx} and q_{Ty} distributions of $J/\psi + \gamma$ final states in two coordinate systems (See text) for a sample with no acceptance cuts and one with ATLAS cuts applied.

noting is the "hole" in mass range 3, leading to a ring shape. This feature presented itself as the loss of gaussianity in Fig. 4b. The remaining two columns show the distribution of events after rotating the x direction such that it aligns with the J/ψ or the photon momentum. Overall, we can observe a shift along the x axis (towards positive values for J/ψ and contrary for the photon), a compression of the width along x and an elongation along y. The x-shift and width varies between the different mass ranges, whereas the width of the y-component changes much slower with invariant mass. The most drastic effects can be seen in the lowest mass range, where big patches of momentum space are left with no events.

The main result of this exercise is showing that choosing a non-arbitrary direction for each event allows us to observe a significant change in the resulting distribution, with a significant difference in the behaviour of the x and y components. Our hope is that doing so can reveal some feature of the distribution which remains unaffected by the acceptance cuts required by ATLAS. This has to be compared with the "true" behaviour of the gluon effects, available in `DS1`.

A comparison is shown in Figure 9, where we chose the J/ψ direction to define x. The resulting x and y components of q_T are shown separately. Due to a significant asymmetry between the left and right side of the peak in x (espiecially in Range 3) in the J/ψ frame, we chose to use only the left side for our Gaussian fit. In `DS1`, many of the effects of rotating the frame of reference described previously can also be seen. There is a shift in x (no shift in y), a compression of the x-width and an elongation of the y-width. What differs is the severity of these effects. The peak of the rotated distribution in `DS2` moves by $3-4$ GeV, whereas the original distribution moves only by about 1 GeV. This is an indication that the true shift of the rotated distributions is magnified by acceptance cuts and as such it cannot help us find the gluon distributions encoded in `DS1`. The reduction of width of x in the rotated distribution appears more promising, as p_2 is similar between both data sets in Range 3 (2.5 ± 0.1 GeV and 2.3 ± 0.0 GeV[3], respectively). The same cannot be said about higher mass ranges.

From now on we refer to the p_T of the J/ψ as P_1 and the γ p_T as and P_2, respectively. It is easy to show that (See Appendix A):

$$q_{1x} = P_1 - P_2 + \frac{P_2}{2}\epsilon^2, \tag{11}$$

where q_{1x} is the projection of q_T onto the direction of J/ψ. Analogous equation can be found for q_{2x}, the projection onto γ, where P_1 and P_2 swap places. The directions perpendicular to those naturally form the y components q_{1y} and q_{2y}. If $\Delta\phi$ is the open angle between the two particles, ϵ is defined through $\Delta\phi + \epsilon = \pi$ and can be expected to be small.

We have seen that projecting the final state onto a special direction can change the distribution of q_{Tx} significantly whilst the perpendicular direction remains a Gaussian centered around 0, with an increased width. Per Equation 11, the x component contains information about the magnitude imbalance ($P_1 - P_2$) as well as the angular imbalance (ϵ) between the two final state particles. These two components can lead to a non-zero total q_T and therefore represent the two ways for the

[3] Any error quoted as ± 0.0 GeV means simply that the error is smaller than 0.05 GeV

transverse momentum of gluons to manifest itself in the final state at low q_T. In the following section, we explore one more orientation of the coordinate system in an event. It allows us to separate the magnitude and angular imbalance between its two perpendicular directions.

3.4 The A-and-B split as a way of obtaining f_1^g

The last orientation takes advantage of the almost back-to-back requirement for the momenta of the two final particles, resulting in small ϵ. Consider:

$$\begin{aligned}
\mathbf{q_T}^2 &= (\mathbf{P_1} + \mathbf{P_2})^2 \qquad (12)\\
&= P_1^2 + P_2^2 + 2P_1P_2\cos(\Delta\phi), \qquad \text{with } \epsilon = \pi - \Delta\phi\\
&= P_1^2 + P_2^2 - 2P_1P_2\cos(\epsilon),\\
&\approx P_1^2 + P_2^2 - 2P_1P_2(1 - \frac{\epsilon^2}{2}), \qquad (\epsilon \text{ is small})\\
&\approx (P_1 - P_2)^2 + P_1P_2\sin\epsilon^2,\\
&= A^2 + B^2, \qquad (13)
\end{aligned}$$

where $A = P_1 - P_2$ is the difference in magnitudes, i.e. the magnitude imbalance and $B = \sqrt{P_1P_2}\sin\epsilon$ contains information about angular imbalance. This separation allows for a more intuitive understanding of the behaviour of these two perpendicular distributions. This configuration is symmetric under the exchange of P_1 and P_2. B bisects the opening angle. Figure 10 shows the final state in that frame.

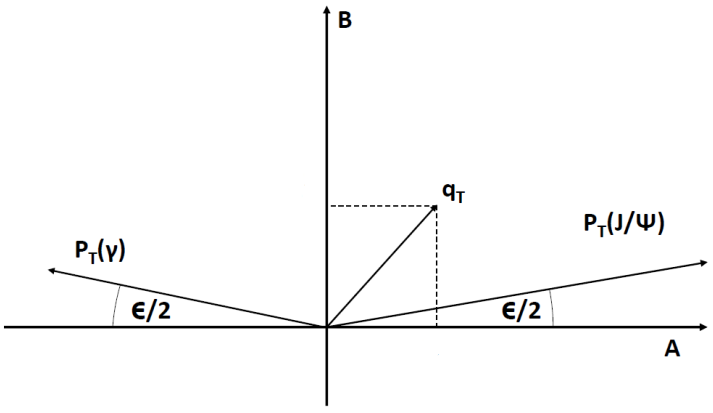

Figure 10: The A-and-B coordinate system used to extract gluon momenta from the $J/\psi + \gamma$ final state. ϵ is expected to be small.

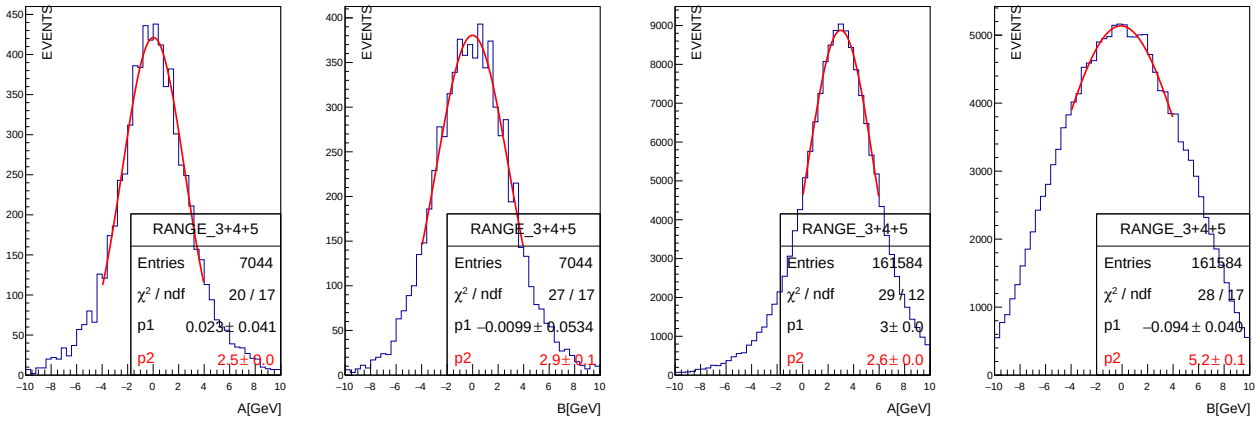

(a) Ideal detector. (b) After applying realistic acceptance cuts.

Figure 11: A and B components of the $q_T \approx \sqrt{A^2 + B^2}$ split before and after applying realistic acceptance cuts. All mass ranges used for the analysis of $J/\psi + \gamma$ final states are combined.

By performing a comparison of A and B between `DS1` and `DS2` we obtained a promising result. Figure 11 shows the two components in the two samples without splitting the events by their invariant mass. As A corresponds to momentum imbalance, it gains a shift in the positive direction. This reflects the asymmetry of the 4/4/5 GeV cut. The width, however, remains *unchanged* between the two samples. In `DS1`, the width of A matches that of q_T. This means that the measurement of A in a real experiment would be equivalent to the measurement of the true q_T width and hence could serve to determine f_1^g. B, on the other hand, gets much wider around the peak, which in both cases coincides with 0 GeV. As small momenta of the J/ψ and γ are excluded, their product $P_1 P_2$ never becomes small and a lot of events around the peak are lost.

Analysing A in the three mass ranges (Fig. 12) reveals that Range 4 does not seem to retain its width well. This is not well understood at the moment and should be addressed by future analyses. Events with lowest Qs are the ones dominating the statistics and hence the overall behaviour when the three ranges are combined. This can be interpreted as motivation to abandon the mass range split in the real analysis and focus on either analysing data in mass bin 3 or in all bins combined (for better statistics).

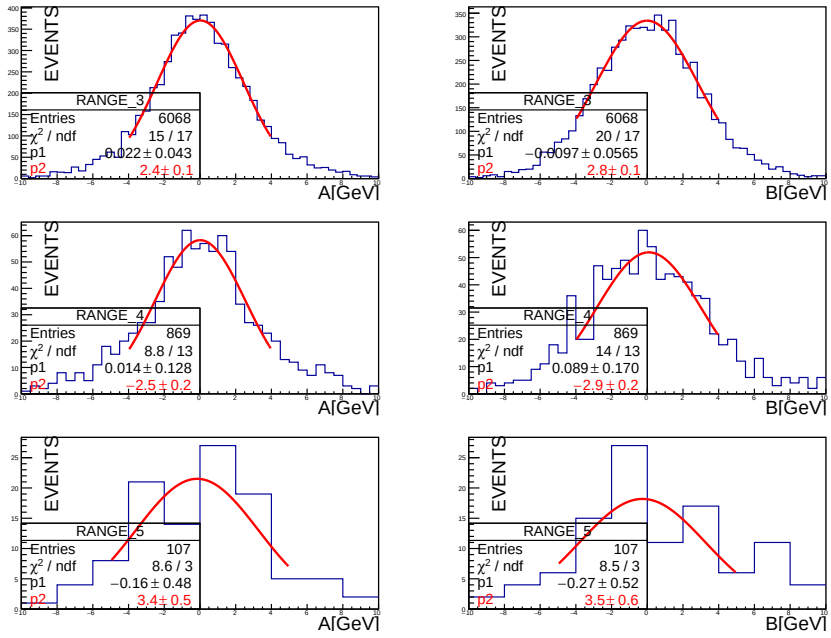

(a) Ideal detector.

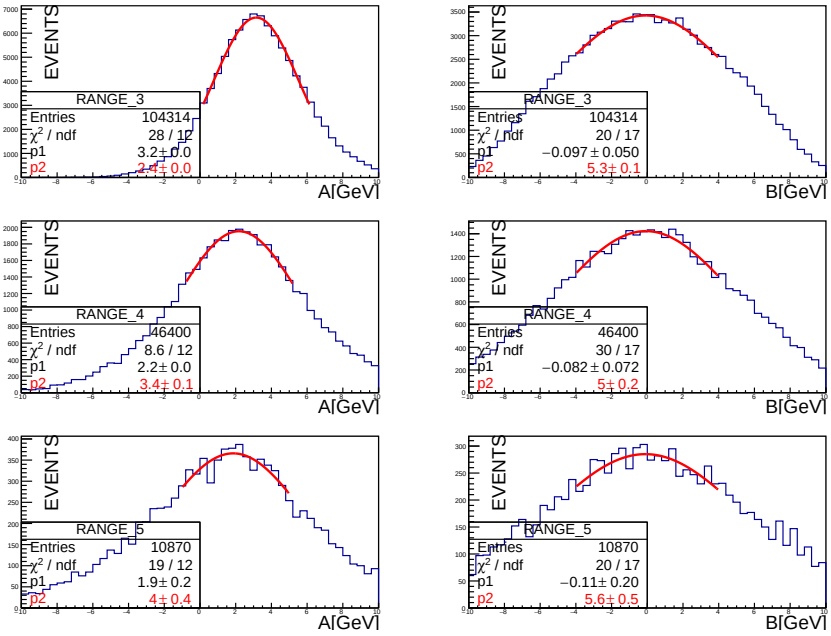

(b) After applying realistic acceptance cuts.

Figure 12: A and B components of the $q_T \approx \sqrt{A^2 + B^2}$ split before and after applying realistic acceptance cuts. Data presented for three separate $J/\psi + \gamma$ final state mass bins.

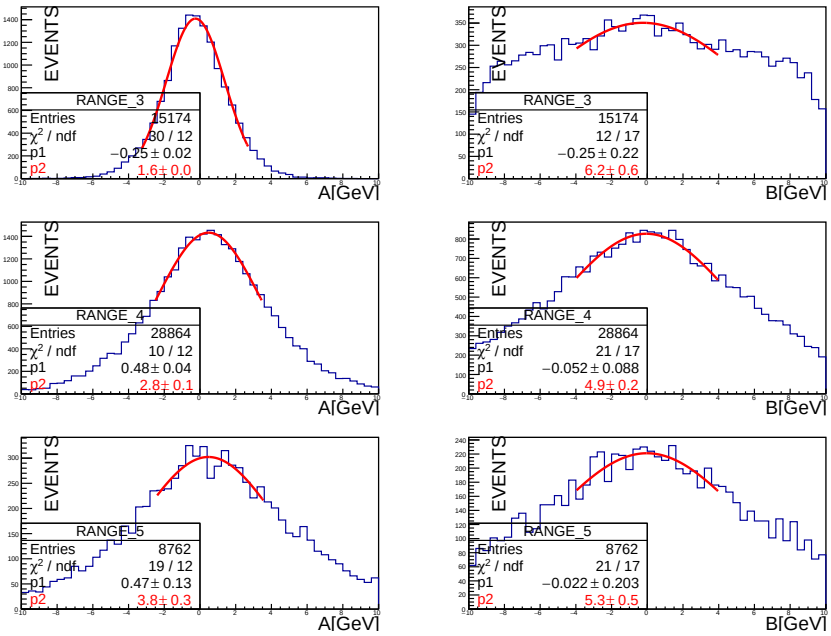

Figure 13: A and B components of the $q_T \approx \sqrt{A^2 + B^2}$ split when acceptance cuts on the $J/\psi + \gamma$ final state transverse momenta are made roughly symmetric (4/4/9 GeV).

The effects of applying balanced acceptance cuts (4/4/9 GeV) can be seen in Figure 13. A at low masses becomes squeezed (understandably, as bringing the values of P_1 and P_2 close leaves less possibilities for their difference to be large). Higher invariant masses have changed less significantly between 4/4/5 GeV and 4/4/9 GeV. The B-component in Range 3 is extremely distorted, resulting in a nearly-flat distribution. We visualise the distribution of both A and B versus invariant mass in Fig. 14. Some empty regions can be seen. These were avoided when producing fits to the data with 4/4/5 GeV cuts, but were included in fits to data with balanced cuts. This helps us understand why Range 3 in Fig. 13 appears to be so strongly distorted. These empty regions correspond to events lost due to the high photon acceptance cut. This further suggests that if A is to be extracted, it should be analysed either at low acceptance cuts or at higher mass ranges, possibly combined. One could reduce the range of the fit to A, such that the empty regions are not included, in hope to recover a less distorted width. In what follows, however, we focus on the most promising result so far, the fit to A in Range 3 for 4/4/5 GeV acceptance cuts.

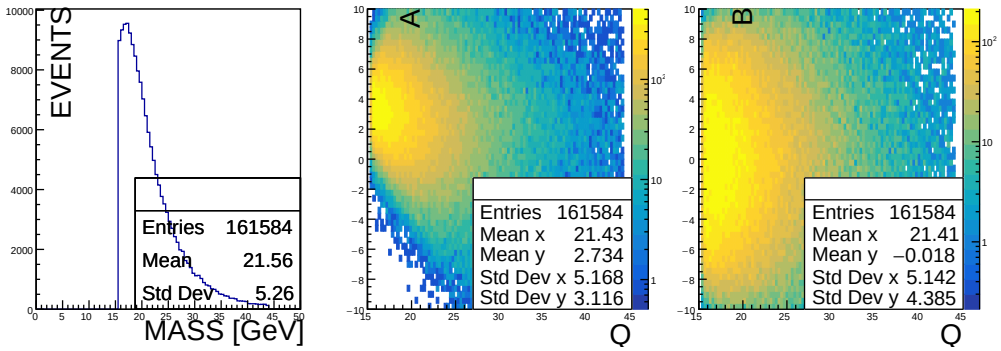

(a) 4/4/5 GeV acceptance cuts on transverse momenta of the final state applied.

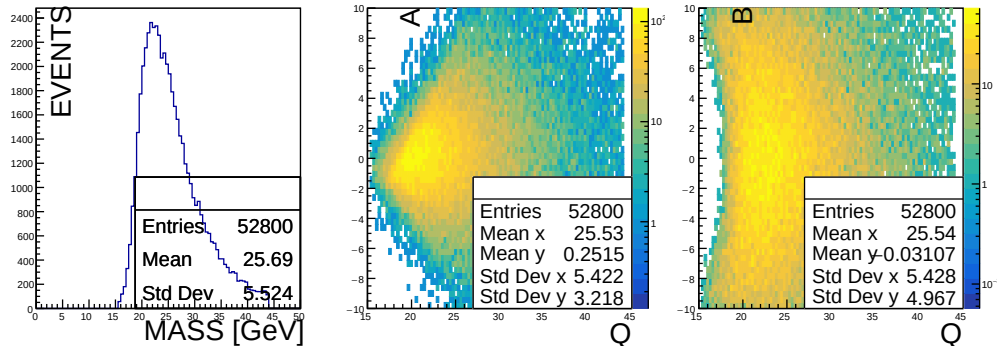

(b) 4/4/9 GeV acceptance cuts on transverse momenta of the final state applied.

Figure 14: A and B distributions in $J/\psi + \gamma$ final states vs their invariant mass Q. Axes given in GeV in the two last columns.

3.5 Event weighting

As the comparison between the two samples so far boils down to comparing *one* parameter, it is possible that their values are the same simply by chance. The combined muon and photon cuts could happen to cancel each other out in a way that produces the same width between the two MC samples. It is not guaranteed that the same would happen for a different width of the q_T distribution. To tackle this problem, one could change the initial distribution of gluons encoded in the event generator and produce the two data sets again. If, for *any* internal gluon distribution, the two numbers match, then one can be sure that A indeed carries that information through to the realistic `DS2`. Unfortunately, producing Monte Carlo samples takes a long time and tweaking with the physics encoded inside is not a trivial task. Instead, we can *artificially* change effects of the gluon distribution by applying weights to the distribution of q_T in `DS1`. This exploits the immediate correspondence between the gluon distribution and the distribution of q_T via $p_2^2 = \langle k_T^2 \rangle$ in `DS1`.

To do so, we first fit the original distribution with a function $\mathcal{F}(q_T)$ given by Equation 9, but with the shift parameter forced to 0 GeV to avoid large errors, as described previously. This results in $p_2 \approx 2.5\,\text{GeV}$. Then we produce another function $\mathcal{F}'(q_T)$ given by the same formula yet with a smaller width parameter p_2'. The weight is obtained by

$$\mathcal{F}_w(q_T) = \frac{\mathcal{F}'(q_T)}{\mathcal{F}(q_T)}. \tag{14}$$

This results in a Gaussian weight:

$$\mathcal{F}_w(q_T) = \exp\left(-\frac{1}{2}\frac{q_T^2}{p_w^2}\right), \tag{15}$$

where $p_w = \frac{p_2 p_2'}{\sqrt{p_2^2 - p_2'^2}}$. The original q_T distribution weighted with $\mathcal{F}_w(q_T)$ will return a distribution described by $\mathcal{F}'(q_T)$. All other distributions (like q_{Tx}, A, B) will act as if the original q_T distribution was given by $\mathcal{F}'(q_T)$ as well. Thus we can treat this as an artificial change of the original distribution of gluons. Figure 15 shows results of weighting each event in `DS1` with $\mathcal{F}_w(q_T) = \exp\left(-\frac{1}{2}\frac{q_T^2}{(3.33)^2}\right)$, which brings down p_2 of the original q_T distribution to 2. Figure 16 shows the same weight being applied to `DS2` hence propagating the effect of the "new gluon distribution" to our realistic sample. Promisingly, the width of A (mass range 3) in both weighted distributions is the same, best fitted with $p_2 = 1.8\pm \approx 0.1\,\text{GeV}$ and $\chi^2/d.o.f \approx 1$. It is worth noting that the shift of A in `DS2` becomes smaller when the average gluon momentum encoded in the width of q_T in `DS1` decreases, and if the relation between the two was found, this could also be used as an alternative way of obtaining f_1^g. Table 2 compares widths of all the weighted distributions plotted in Figures 15 and 16. A in mass range 3 is the only variable with a confident fit (relatively small error) which retains its distribution between the two weighted data sets. This provides evidence that it could indeed be avoiding the detector acceptance effects and did not produce promising results by pure chance.

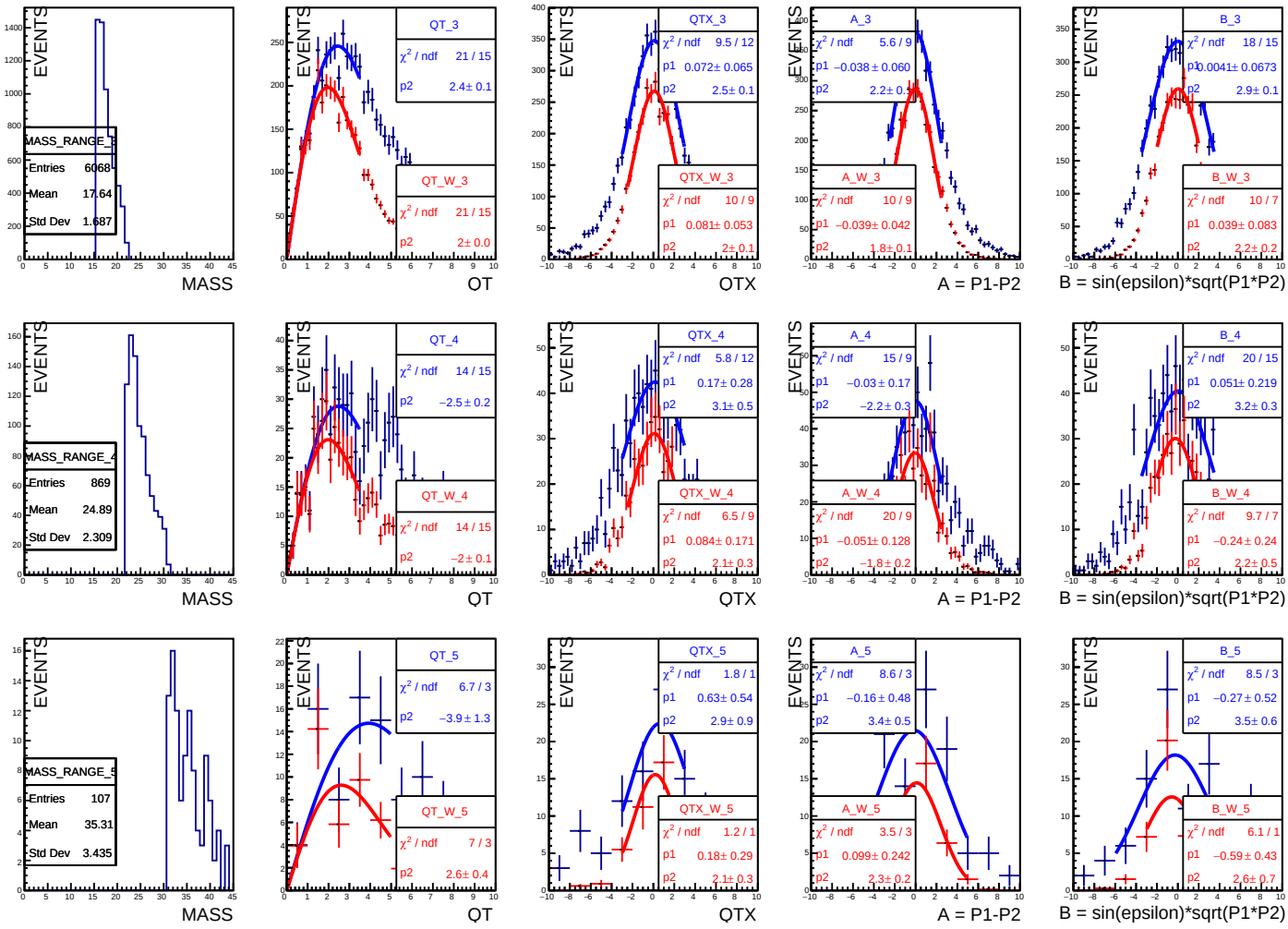

Figure 15: Effects of artificially changing the distribution of $J/\psi + \gamma$ q_T ($p_2 \approx 2.5 \rightarrow 2\,\mathrm{GeV}$) on an ideal detector data set. Related distributions are shown, including the A and B components. Horizontal axes given in GeV.

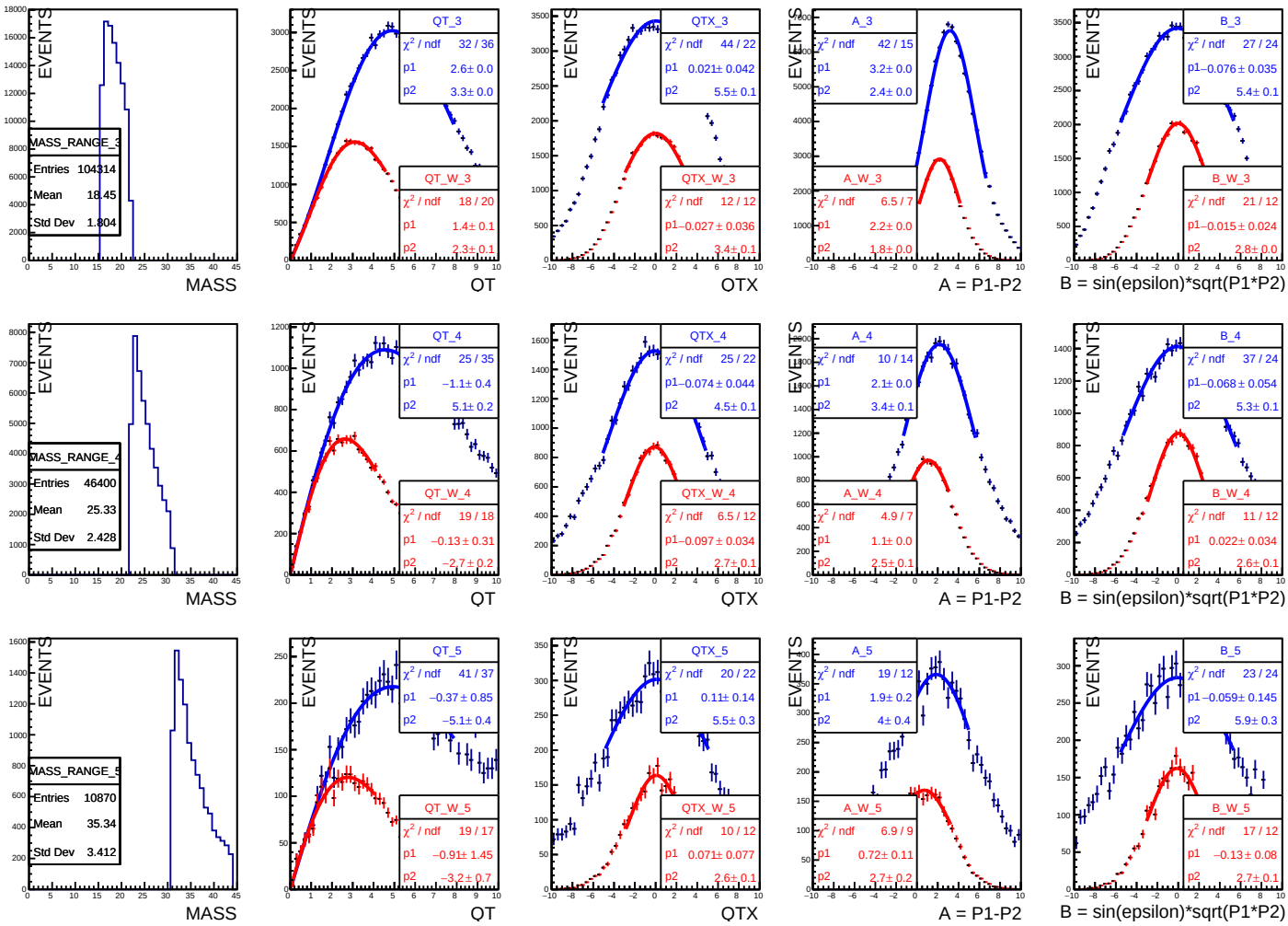

Figure 16: Effects of artificially changing the distribution of $J/\psi + \gamma$ q_T ($p_2 \approx 2.5 \rightarrow 2\,\mathrm{GeV}$) in an ideal detector data set, propagated to a sample with acceptance cuts. Related distributions are shown, including the A and B components. Horizontal axes given in GeV.

	Mass range 3		Mass range 4		Mass range 5	
	DS1	DS2	DS1	DS2	DS1	DS2
q_T	1.97 ± 0.04	2.33 ± 0.06	-1.99 ± 0.12	-2.69 ± 0.16	2.61 ± 0.40	-3.19 ± 0.71
q_x	1.97 ± 0.08	3.38 ± 0.08	2.11 ± 0.29	2.67 ± 0.06	2.10 ± 0.33	2.61 ± 0.13
A	1.76 ± 0.06	1.84 ± 0.03	-1.81 ± 0.17	2.46 ± 0.12	2.33 ± 0.18	2.74 ± 0.24
B	2.21 ± 0.18	2.80 ± 0.04	2.16 ± 0.52	2.60 ± 0.05	2.60 ± 0.70	2.73 ± 0.15

Table 2: Widths of distributions in $J/\psi + \gamma$ data related to q_T compared between the ideal simulation DS1 and DS2, where acceptance cuts are applied. Events have been weighted to artificially change the distribution of q_T in DS1. All values given in GeV.

Figure 17 shows the ratios of the widths of A and B in the two data sets for 6 different weights applied. These correspond to values of the new "true" q_T distribution ranging from 2.4 GeV to 1.4 GeV in equal steps.

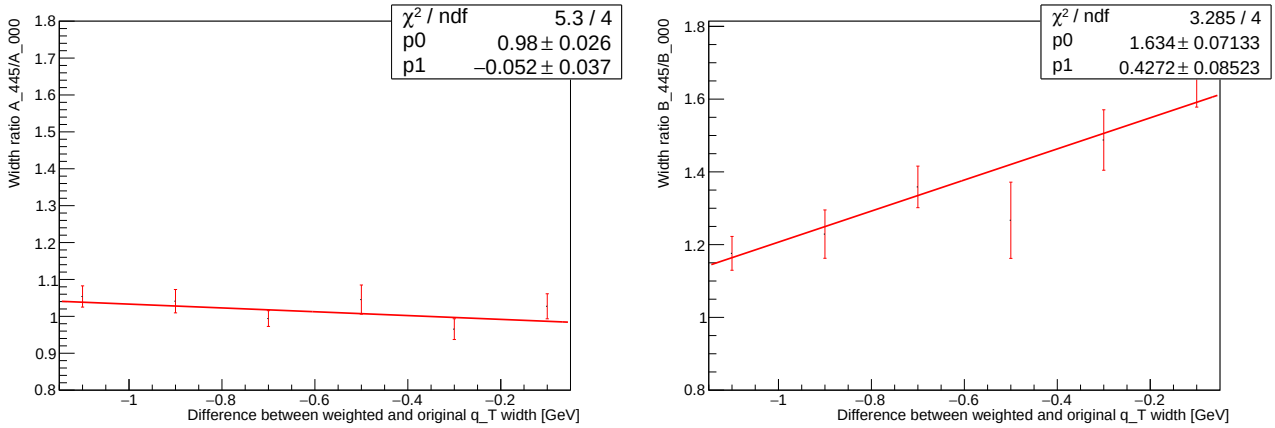

(a) A-component of q_T.

(b) B-component of q_T.

Figure 17: Ratio of widths in a realistic data set to widths in an ideal one for different weights applied to the $J/\psi + \gamma$ data. These correspond to different effective distributions of the original q_T. The original width was taken as 2.5 GeV. Note that error bars shown are likely too big, as no correlation of data points was used in their calculation even though they come from the same distribution.

The ratios are fitted with a linear function where the p_0 parameter indicates the constant and p_1 is the slope. These are both consistent with a constant ratio of 1 for A. p_0 within one and p_1 within two standard deviations. This is exactly what we hoped for and is the most important result of our analysis. B shows significant broadening throughout, as expected. What is promising, however,

is the good fit to a simple linear relationship. This means that if the relation of B to q_T before acceptance cuts is understood, a measurement of B could also be used to obtain f_1^g.

It is worth noting that we assumed that A and q_T are described by the same width originally, yet Table 2 shows that in the weighted case there is a small difference between the fits to the two. Whether this is a result of choosing a fit range that is too wide or a result of the approximation $q_T^2 \approx A^2 + B^2$ breaking is unknown at the moment. Nonetheless, measuring A remains the best estimation of the original q_T that has been found in this analysis.

4 Future Work

The LHC Run 2 lasted between 2015 and 2018. The average number of interactions in one bunch crossing has nearly doubled between 2015 and 2016 and increased even more in the following years [37]. This meant that the triggers had to deal with more and more data at once (big *pile-up*). To cope with that, the two-muon trigger had to be raised from 4 to 6 GeV. This has to be accounted for if this analysis is to be carried through to the full Run 2 data set. This section provides preliminary results for future, more complete studies of $J/\psi + \gamma$ at ATLAS. We apply 6/6/10 GeV cuts on `DS2`. The choice to raise the photon acceptance to 10 GeV is motivated by the fact that for the Run 2 data, efficiency maps exist for photons beginning at 10 GeV [40].

Figure 18 shows what happens to our sample. Only about 0.073% of events from the 4/4/5 GeV cut survive in mass range 3. No low q_T events survive and hence the events in this range do not satisfy the factorisation condition $q_T \ll Q$, given that Q peaks around 20 GeV and the peak of q_T is around 13 GeV. We still manage to get a fit for A, which has now shrunk to 1.0 ± 0.2 GeV. We have previously seen shrinking in this mass range caused by applying a 9 GeV photon cut in Section 3.4. Mass range 4 retains about 7.3% of events and the width of A now matches that of the original distribution in `DS1`. A further investigation analogous to that presented in Section 3.5 could help determine whether this is a promising mass range for the extraction of f_1^g in the full 2015-2018 ATLAS data set. Mass range 5 lost 72% of events and the shape of its mass distribution has been affected the least. As a consequence, the shapes of all other distributions in this range are consistent with the results for the 2015-based cuts, albeit with larger errors due to smaller statistics. The increased integrated luminosity of the full Run 2 will compensate the statistics losses from higher cuts. The 2015 data comprises less than 3% of the full Run 2 sample [44]. Thus, assuming a uniform increase throughout mass ranges, one could expect roughly (3%, 250%, 900%) of events in Ranges (3, 4, 5) with respect to the numbers obtained in 2015 alone. This would be a great improvement in overall statistics. Ranges 3 and 4 could be combined for highest possible statistics and to avoid including the empty regions from acceptance cuts, a range of ± 2 GeV around the peak could be used to determine the width of the distribution. Provided that the shape of Range 4 reacts to the distribution of gluons just like Range 3 did in our analysis in Section 3.5 (Fig. 17a), the full Run 2 ATLAS data on $J/\psi + \gamma$ could be used for a more precise extraction of the gluon distribution function f_1^g.

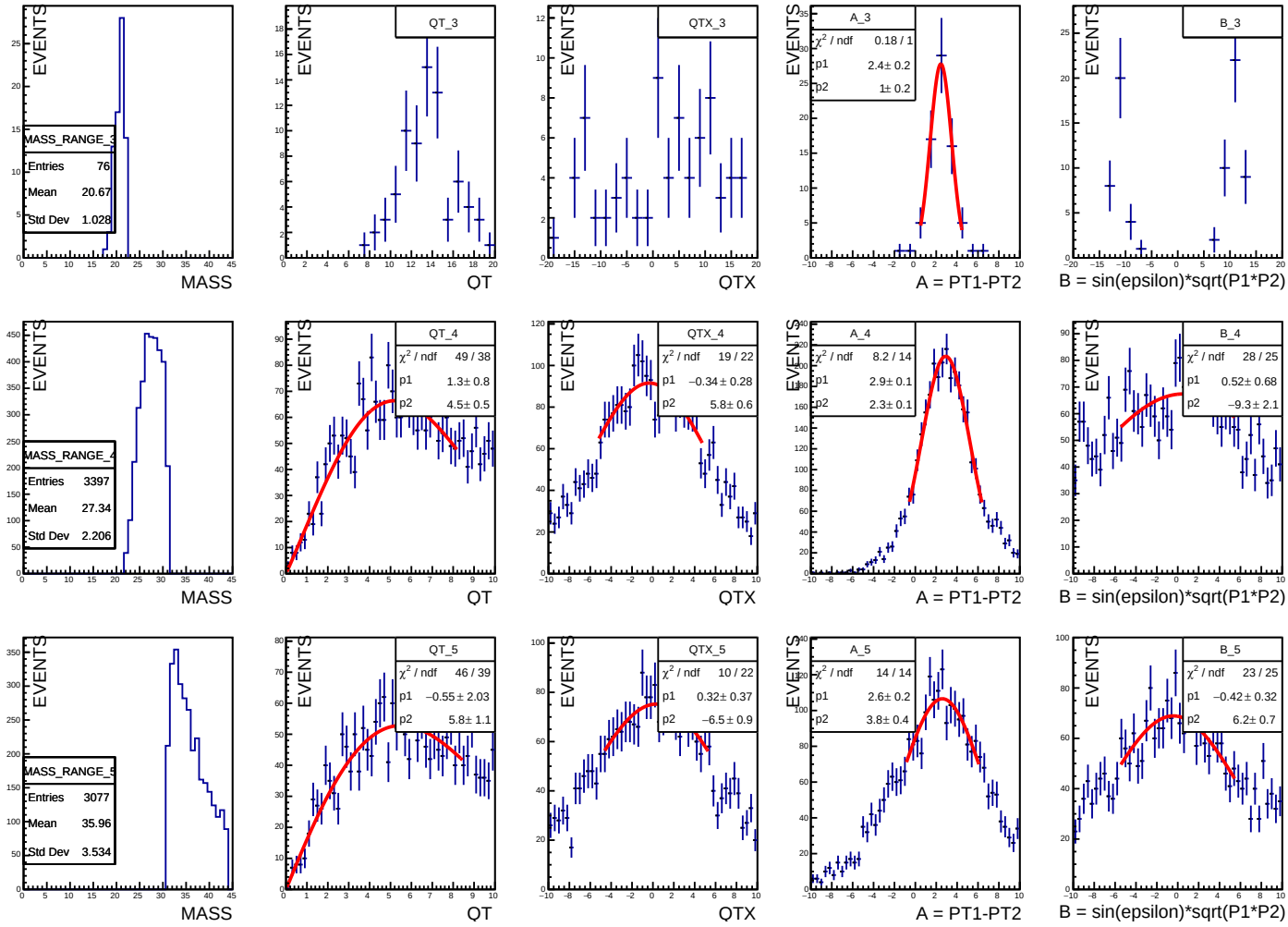

Figure 18: q_T of $J/\psi + \gamma$ pair and related distributions after acceptance cuts are applied. These are required to analyse ATLAS data from the full LHC Run 2.

5 Conclusions

Strong theoretical arguments suggest that the $J/\psi + \gamma$ final state in proton-proton collisions at high energies can be used to find a transverse momentum dependent distribution function of gluons f_1^g. This thesis focused on taking these theoretical predictions closer to an extraction from real-world, experimental data.

Monte Carlo simulated events were used to show how the ATLAS detector acceptance cuts affect the final state data (Section 3.2). The width of the distribution of the final state transverse momentum q_T yields information about f_1^g. This width was shown to be broadened significantly by acceptance effects, obscuring the information required for extraction. Methods of mitigating these effects were searched for, exposing properties of the final state and revealing promising results. Rotating the coordinate system in which q_T is measured changes its distribution significantly.

A rotation from the laboratory frame to one which bisects the opening angle between J/ψ and γ (Section 3.4), approximately separates the magnitude and the angular imbalance, which together lead to a non-zero q_T. They become encoded on the two perpendicular directions of the coordinate system. One of those, which we call "A" appears to resist acceptance cuts effects, by retaining the width of its distribution. The other, dubbed "B", shows significant broadening. When combined to form q_T, the behaviour of B dominates.

By artificially changing the underlying gluon distribution (Section 3.5), A was shown to remain unaffected by the acceptance cuts, ruling out the possibility of a matching width obtained by pure chance. The linear relation found for B after cuts are applied on the underlying gluon distribution could also help verify any results obtained with A.

Some predictions were made for the behaviour of the final state in future analyses, which will use data from the full Run 2 at the LHC (Section 4). A likely remains a good probe of the gluon transverse momentum even after more rigorous acceptance cuts, required by the new data set, are applied.

A thorough understanding of the relation of A and B to q_T ("How good is the approximation $q_T^2 \approx A^2 + B^2$?"), and an analysis of background events and their subtraction in real data are still needed if an extraction of f_1^g is to be made. Additionally, the evolution of widths in the data with mass Q is not currently well understood, given that the "true" sample produced slow-varying distributions between the mass ranges explored. Choosing a range of masses that maximises statistics whilst reflecting the underlying behaviour of gluons will be crucial.

The work presented in this thesis, however, shed some light on the properties of $J/\psi + \gamma$ in the context of gluon transverse momenta and motivated a shift away from a direct measurement of the distribution of q_T and onto an analysis in the A-and-B coordinate system.

Potentially worth noting is the result from Section 3.3, where the width of the x-distribution aligned with J/ψ in Range 3 appeared almost unchanged between the two data sets. Further analysis, similar to that presented for A in this report, could help determine the usefulness of that variable in extraction of gluon TMDs.

References

[1] CERN [Internet]. CERN. The Large Hadron Collider; [cited 2021 Apr 15]. Available from: https://home.cern/science/accelerators/large-hadron-collider

[2] Cern LHC sees high-energy success. BBC News [Internet]. 2010 Mar 30 [cited 2021 Apr 15]. Available from: http://news.bbc.co.uk/1/hi/sci/tech/8593780.stm

[3] CERN [Internet]. CERN. Long term LHC schedule; [cited 2021 Apr 15]. Available from: https://lhc-commissioning.web.cern.ch/schedule/LHC-long-term.htm

[4] CERN [Internet]. CERN. High-Luminosity LHC; [cited 2021 Apr 15]. Available from: https://home.cern/science/accelerators/high-luminosity-lhc

[5] den Dunnen W, Lansberg J, Pisano C, Schlegel M. Accessing the Transverse Dynamics and Polarization of Gluons inside the Proton at the LHC. Physical Review Letters. 2014;112(21). DOI: 10.1103/PhysRevLett.112.212001

[6] LHCb collaboration: Aaij R, Abellán Beteta C, Ackernley T, Adeva B, Adinolfi M, Afsharnia H. Observation of new resonances decaying to $J/\psi K^+$ and $J/\psi\phi$ Available from: https://arxiv.org/abs/2103.01803

[7] Gell-Mann M. A Schematic Model of Baryons and Mesons. Resonance. 2019;24(8):923-925. DOI: 10.1007/s12045-019-0853-x

[8] Martin BR, Shaw G. Particle Physics. New York: John Wiley & Sons, Incorporated; 2017. Chapter 6, The quark model; p. 156-162.

[9] Sterman G, Smith J, Collins J, Whitmore J, Brock R, Huston J et al. Handbook of perturbative QCD. Reviews of Modern Physics. 1995;67(1):157-248. DOI: 10.1103/RevModPhys.67.157

[10] Tanabashi M, Hagiwara K, Hikasa K, Nakamura K, Sumino Y, Takahashi F et al. Quantum Chromodynamics. Review of Particle Physics. Physical Review D. 2018;98(3). DOI:10.1103/PhysRevD.98.030001

[11] Collins J, Soper D, Sterman G. Factorization of hard processes in QCD. Perturbative QCD. 1989;:1-91. DOI: 10.1142/9789814503266_0001

[12] Collins J, Qiu J. k_T factorization is violated in production of high-transverse-momentum particles in hadron-hadron collisions. Physical Review D. 2007;75(11). DOI: 10.1103/PhysRevD.75.114014

[13] Buffing MGA, Color and TMD universality in hadronic interactions [PhD thesis]. Amsterdam, NIKHEF, 2015.

[14] Soper D. Parton distribution functions. Nuclear Physics B - Proceedings Supplements. 1997;53(1-3):69-80. DOI: 10.1016/S0920-5632(96)00600-7

[15] Constantinou M, Courtoy A, Ebert MA, Engelhardt M, Giani T, Hobbs T et al. Parton distributions and lattice QCD calculations: toward 3D structure. Available from: https://arxiv.org/abs/2006.08636

[16] Petreska E. TMD gluon distributions at small x in the CGC theory. International Journal of Modern Physics E. 2018;27(05):1830003. DOI: 10.1142/S0218301318300035

[17] Angeles-Martinez R, Bacchetta A, Balitsky I, Boer D, Boglione M, Boussarie R et al. Transverse Momentum Dependent (TMD) Parton Distribution Functions: Status and Prospects. Acta Physica Polonica B. 2015;46(12):2501. 10.5506/APhysPolB.46.2501

[18] Boer D, den Dunnen W, Pisano C, Schlegel M, Vogelsang W. Linearly polarised Gluons and the Higgs Transverse Momentum Distribution. Physical Review Letters. 2012;108(3). DOI: 10.1103/PhysRevLett.108.032002

[19] Tanabashi M, Hagiwara K, Hikasa K, Nakamura K, Sumino Y, Takahashi F et al. Structure Functions. Review of Particle Physics. Physical Review D. 2018;98(3). DOI:10.1103/PhysRevD.98.030001 DOI:10.1103/PhysRevD.98.030001

[20] Lansberg J, Pisano C, Schlegel M. Associated production of a dilepton and a $\Upsilon(J/\psi)$ at the LHC as a probe of gluon transverse momentum dependent distributions. Nuclear Physics B. 2017;920:192-210.

[21] Mulders P, Rodrigues J. Transverse momentum dependence in gluon distribution and fragmentation functions. Physical Review D. 2001;63(9). DOI: 10.1103/PhysRevD.63.094021

[22] Metz A, Zhou J. Distribution of linearly polarized gluons inside a large nucleus. Physical Review D. 2011;84(5). DOI:10.1103/PhysRevD.84.051503

[23] Lansberg J, Pisano C, Scarpa F, Schlegel M. Pinning down the linearly-polarised gluons inside unpolarised protons using quarkonium-pair production at the LHC. Physics Letters B.791 (2019) 420-42 (erratum) DOI: 10.1016/j.physletb.2019.01.057

[24] Echevarría M, Idilbi A, Scimemi I. Factorization theorem for Drell-Yan at low q_T and transverse-momentum distributions on-the-light-cone. Journal of High Energy Physics. 2012;2012(7). DOI:10.1007/JHEP07(2012)002

[25] Echevarría M, Idilbi A, Scimemi I. Soft and collinear factorization and transverse momentum dependent parton distribution functions. Physics Letters B. 2013;726(4-5):795-801. DOI: 10.1016/j.physletb.2013.09.003

[26] Pisano C, Boer D, Brodsky S, Buffing M, Mulders P. Linear polarization of gluons and photons in unpolarized collider experiments. Journal of High Energy Physics. 2013;2013(10). DOI: 10.1007/JHEP10(2013)024

[27] DESY Home [Internet]. Deutsches Elektronen-Synchrotron DESY. HERA; [cited 2021 Apr 16]. Available from: https://www.desy.de/research/facilities__projects/hera/index_eng.html

[28] RHIC [Internet]. Brookhaven National Laboratory, the Relativistic Heavy Ion Collider. The Physics of RHIC; [cited 2021 Apr 16]. Available from: https://www.bnl.gov/rhic/physics.asp

[29] Chekanov S, Derrick M, Magill S, Musgrave B, Nicholass D, Repond J et al. Multijet production at low in deep inelastic scattering at HERA. Nuclear Physics B. 2007;786(1-2):152-180. Available from: 10.1016/j.nuclphysb.2007.05.027

[30] Qiu J, Schlegel M, Vogelsang W. Probing Gluonic Spin-Orbit Correlations in Photon Pair Production. Physical Review Letters. 2011;107(6). DOI: 10.1103/PhysRevLett.107.062001

[31] Boer D, Pisano C. Polarized gluon studies with charmonium and bottomonium at LHCb and AFTER. Physical Review D. 2012;86(9). DOI: 10.1103/PhysRevD.86.094007

[32] Drees M, Kim C. Associate $J/\psi + \gamma$ production: a clean probe of gluon densities. Zeitschrift für Physik C Particles and Fields. 1992;53(4):673-678. DOI: 10.1007/BF01559746

[33] Coffman D, Dubois G, Eigen G, Hauser J, Hitlin D, Matthews C et al. Measurements of J/ψ decays into a vector and a pseudoscalar meson. Physical Review D. 1988;38(9):2695-2705. DOI: 10.1103/PhysRevD.38.2695

[34] Collins J, Soper D. Angular distribution of dileptons in high-energy hadron collisions. Physical Review D. 1977;16(7):2219-2225. DOI: 10.1103/PhysRevD.16.2219

[35] Schweitzer P, Teckentrup T, Metz A. Intrinsic transverse parton momenta in deeply inelastic reactions. Physical Review D. 2010;81(9). DOI: 10.1103/PhysRevD.81.094019

[36] CERN [Internet]. CERN. First images of collisions at 13 TeV; [cited 2021 Apr 25]. Available from: Available from: https://home.cern/news/news/accelerators/first-images-collisions-13-tev

[37] Aaboud M, Aad G, Abbott B, Abdallah J, Abdinov O, Abeloos B et al. Performance of the ATLAS trigger system in 2015. The European Physical Journal C. 2017;77(5). DOI: 10.1140/epjc/s10052-017-4852-3

[38] ATLAS collaboration. Muon reconstruction and identification efficiency in ATLAS using the full Run 2 pp collision data set at $\sqrt{s} = 13$ TeV Available from: https://inspirehep.net/literature/1809957

[39] Aad G, Abbott B, Abbott D, Abud A, Abeling K, Abhayasinghe D et al. Performance of the ATLAS muon triggers in Run 2. Journal of Instrumentation. 2020;15(09):P09015-P09015. DOI: 10.1088/1748-0221/15/09/p09015

[40] Aaboud M, Aad G, Abbott B, Abdinov O, Abeloos B, Abhayasinghe D et al. Measurement of the photon identification efficiencies with the ATLAS detector using LHC Run 2 data collected in 2015 and 2016. The European Physical Journal C. 2019;79(3). DOI: 10.1140/epjc/s10052-019-6650-6

[41] Sjöstrand T, Ask S, Christiansen J, Corke R, Desai N, Ilten P et al. An introduction to PYTHIA 8.2. Computer Physics Communications. 2015;191:159-177. DOI: 10.1016/j.cpc.2015.01.024

[42] Tee A. A Gluon Transverse Momentum Dependent Parton Distributuon Function Analysis Using a Final State $J/\psi + \gamma$ at $\sqrt{s} = 13\,\text{TeV}$ With ATLAS. Lancaster (UK): Lancaster University; 2021 [cited 2021 Apr 17]. Available from: https://cds.cern.ch/record/2750054?ln=en

[43] Caola F, Forte S, Rojo J. HERA data and DGLAP evolution: Theory and phenomenology. Nuclear Physics A. 2011;854(1):32-44. DOI: 10.1016/j.nuclphysa.2010.08.009

[44] ATLAS collaboration. Luminosity determination in pp collisions at $\sqrt{s} = 13\,\text{TeV}$ using the ATLAS detector at the LHC. Available from: https://inspirehep.net/literature/1737864

A Projection on J/ψ

$$\begin{aligned} q_{1x} &= P_1 + \mathbf{P_2} \cdot \frac{\mathbf{P_1}}{P_1}, \\ &= P_1 + P_2 \cos(\pi - \epsilon), \\ &= P_1 - P_2 \cos\epsilon, \\ &\approx P_1 - P_2 + \frac{P_2}{2}\epsilon^2, \qquad \text{from } \cos\epsilon \approx 1 - \tfrac{\epsilon^2}{2}. \end{aligned}$$

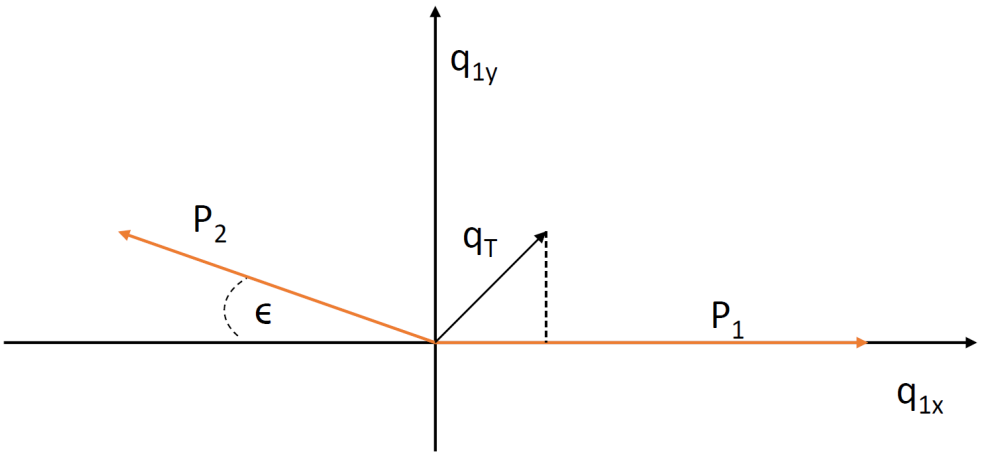

Figure 19: $\mathbf{q_T}$ of the $J/\psi + \gamma$ pair presented in a rotated frame of reference, where the x-component lies along the J/ψ direction.